Dalton Transactions

Accepted Manuscript

ROYAL SOCIETY OF CHEMISTRY

www.rsc.org/dalton

Dalton Transactions

ARTICLE

Optimization of upconversion luminescence of Nd^{3+}-sensitized $BaGdF_5$-based nanostructures and their application in dual-modality imaging and drug delivery

Received 00th January 20xx,
Accepted 00th January 20xx

DOI: 10.1039/x0xx00000x

www.rsc.org/

Fei He,[a,c] Chunxia Li,[a,*] Xinyang Zhang,[a] Yinyin Chen,[a,c] Xiaoran Deng [a,c] Bei Liu,[a,c] Zhiyao Hou,[a] Shanshan Huang,[a] Dayong Jin [b] and Jun Lin [a,*]

808 nm excited upconversion nanoparticles (UCNPs) have received extensive attention in the biomedical areas. However, one of the limitations of UCNPs is their lower luminescence efficiency. Aimed at this problem, a series of $BaGdF_5$-based UCNPs were prepared by layer-by-layer procedure. And UC luminescence properties are optimized by varying the doping concentration of rare earth ions, amount and types of the shells. It is found that if the amount of core $BaGdF_5$:20%Yb^{3+}/2%Er^{3+} was fixed at 0.5 mmol, the optimized conditions of three shell layers are 0.3 mmol of $BaGdF_5$:10%Yb^{3+}, 0.5 mmol of $BaNdF_5$ and 0.5 mmol of $BaGdF_5$, respectively. Thus the UC luminescence intensity of the resultant nanoparticles $BaGdF_5$:20%Yb^{3+}/2%Er^{3+}@$BaGdF_5$:10%Yb^{3+}@$BaNdF_5$@ $BaGdF_5$ (Er@Yb@Nd@Gd) is enhanced more than four times compared with that of $BaGdF_5$:20%Yb^{3+}/2%Er^{3+}@$BaGdF_5$:10%Yb^{3+}@$BaNdF_5$ (Er@Yb@Nd). To further improve the biocompatibility and applications in biological field, carboxymethyl chitosan (CMC), a type of biocompatible water-transfer agent, was used as capping ligands to modify the surface of Er@Yb@Nd@Gd. Antitumor drug doxorubicin (DOX) was loaded to the CMC-modified Er@Yb@Nd@Gd nanocarriers by electrostatic interaction. The DOX can be selectively released in acidic environment, which shows a pH-triggered drug release behavior. On the other hand, Er@Yb@Nd@Gd nanoparticles have excellent magnetic property due to the presence of Gd components. The T_1-weighted magnetic resonance imaging (MRI) reveals the concentration-dependent brightening effect with longitudinal relaxivity (r_1) as high as 43.77 s^{-1} $(mM)^{-1}$, much higher than that of previous Gd^{3+}-based counterparts. The results indicate that this multifunctional drug delivery system is expected to be a promising platform for simultaneous cancer therapy and bioimaging.

1 Introduction

Solid inorganic fluorides have been of great interest to researchers because of their good chemical stability and low-energy phonons.[1-4] Among these materials, upconversion nanoparticles (UCNPs) have found extensive applications in biomedical areas, such as in vivo imaging,[5-8] bioprobes,[9] drug delivery,[10] gene therapy,[11] photothermal and photodynamic therapy.[12-14] However, one of the limitations of conventional UCNPs is their low conversion efficiency, especially under low-intensity laser excitation. Nowadays, 980 nm laser is the most commonly used NIR excitation source to generate UC emission.[15-21] However, 980 nm laser can be absorbed by water and induce overheating effect, which hinders more applications of 980 nm laser.[19] Nd^{3+}-doped UCNPs excited by 808 nm laser excitation have nearly no overheating effect and can improve this aspect of the upconversion nanomaterials.[22-30] Yao et. al. designed a transition layer into the core-shell structure and constructed a quenching-shield sandwich structure to eliminate photon quenching, which prevent energy back-transfer from activators (Er^{3+},Tm^{3+},Ho^{3+}) to the sensitizer Nd^{3+}.[28]

Meanwhile, magnetic resonance imaging (MRI) modalities are characterized by high sensitivity and good discrimination for soft tissues respectively. Gd^{3+}-based UC have been a popular contrast agent for imaging and diagnosis.[31-33] As is known, Gd^{3+} ion has seven unpaired electrons and could provide high paramagnetic relaxivity.[34-35] The large magnetic moment made them ideal paramagnetic relaxation agents. Therefore, Gd^{3+}-doped UC are magnetic/upconversion nanocomposites with excellent magnetic

[a] State Key Laboratory of Rare Earth Resource Utilization, Changchun Institute of Applied Chemistry, Chinese Academy of Sciences, Changchun 130022, P. R. China. E-mail: cxli@ciac.ac.cn, jlin@ciac.ac.cn
[b] Institute for Biomedical Materials and Devices, Faculty of Science, University of Technology Sydney, NSW, 2007, Australia
[c] University of Chinese Academy of Sciences, Beijing 100049, P. R. China
Electronic Supplementary Information (ESI) available: See DOI: 10.1039/x0xx00000

and optical property. The combination of magnetic and luminescent properties yields the nanoprobe with optical and magnetic resonance (MR) dual-modal imaging simultaneously for real-time visualization.[36] Therefore, UCNPs with multifunctionality could be designed by coating a shell layer on the core[37-40] or encapsulating active components into the host materials.[41-43]

In this work, we prepared Nd^{3+}-doped UC nanocrystals via a high temperature boiling solvent process and try to improve their upconversion luminescence intensity. By varying the doping concentration, amount and types of the shells, we constructed $BaGdF_5$:20%Yb^{3+}/2%Er^{3+}@$BaGdF_5$:10%Yb^{3+}@$BaNdF_5$@$BaGdF_5$(Er@Yb@Nd@Gd) core/shell/shell/shell structured upconversion nanoparticles. Next carboxymethyl chitosan (CMC), a kind of biocompatible polymer, was used to modify Er@Yb@Nd@Gd in order to make them have good solubility in water. The CMC-modified Er@Yb@Nd@Gd can be served as UCL imaging and magnetic resonance agents as well as drug carriers simultaneously for biomedical applications.

2 Experimental Section

2.1 Materials

RE_2O_3 (RE = Gd, Yb, Er, Nd; 99.99%) compounds were purchased from Science and Technology Parent Company of the Changchun Institute of Applied Chemistry. Oleic acid (OA) and 1-octadecene (ODE) were purchased from Aldrich. Trifluoroacetic acid (CF_3COOH) was obtained from Aladdin. Barium carbonate ($BaCO_3$) was purchased from Beijing Chemical Regent Co. Ltd., and carboxymethyl chitosan (CMC) was obtained from XiYa Regent Co. Ltd. Company. Doxorubicin (DOX) was obtained from Nanjing Duodian Chemical Limited Company. $RE(CF_3COO)_3$ and $Ba(CF_3COO)_2$ were prepared according to literature method.[44]

2.2 Synthesis of $BaGdF_5$-based multilayer upconversion nanoparticles $BaGdF_5$:20%Yb^{3+}/2%Er^{3+}@$BaGdF_5$:10%Yb^{3+}@ $BaNdF_5$ @$BaGdF_5$ (Er@Yb@Nd@Gd)

Multilayer nanoparticles were fabricated by layer-by-layer epitaxial growth. First, $BaGdF_5$:20%Yb^{3+}/2%Er^{3+} core was fabricated according to the method developed previously.[44] Then, to prepare the Er@Yb@Nd@Gd nanoparticles, 2 mL of cyclohexane solution containing half of nanoparticles was mixed with OA (10 mL) and ODE (10 mL) and subsequently heated to 150 °C under vacuum for 1 h to remove water and oxygen, and thus to form transparent solution. Next, under the protection of N_2 atmosphere, the reaction temperature was rapidly increased to 310 °C. Simultaneously, each shell $RE(CF_3COO)_3$ and $Ba(CF_3COO)_2$ precursors dissolved in 4 mL of OA/ODE (v:v = 1:1) were successively injected into the above system and maintained at this temperature for 1 h. The obtained nanocrystals were centrifuged and washed by ethanol and cyclohexane for three times, respectively, and finally dispersed in 10 mL of cyclohexane for further use.

2.3 Surface modification of core/shell/shell/shell structured Er@Yb@Nd@Gd (labeled as CMC-Er@Yb@Nd@Gd)

The Er@Yb@Nd@Gd were dispersed in 10 mL of chloroform. Then 2 mL solution of Er@Yb@Nd@Gd/$CHCl_3$ was added to 30 mL of aqueous solution containing 100 mg of CMC. After vigorous stirring overnight, the solution was then ultrasonically treated to generate aqueous-phase dispersed nanoparticles. The water-soluble nanoparticles was centrifuged and washed with water.

2.4. Synthesis of DOX-loaded CMC-Er@Yb@Nd@Gd (labeled as DOX-CMC-Er@Yb@Nd@Gd)

30 mg of CMC-Er@Yb@Nd@Gd was dispersed in 5 mL of water. 5 mg of DOX was added to the above solution and stirred for 48 h at room temperature. The precipitates were separated by centrifugation and washed with water several times until the supernatant solution became colorless.

2.5. In vitro cell viability tests of CMC-Er@Yb@Nd@Gd UCNPs

In vitro cell viability was determined by using HeLa cells. Briefly, HeLa cells were plated out at a density of 5000 cells per well in a 96-well plate and incubated in 5% CO_2 at 37 °C overnight. The free DOX and DOX loaded CMC-Er@Yb@Nd@Gd nanoparticles were added to the medium and incubated for 24 h in 5% CO_2 at 37 °C. The concentrations of nanocomposites were 6.25, 12.5, 25, 50, 100 and 200 μg/mL, respectively, while the concentrations of DOX were 0.78125, 1.5625, 3.125, 6.25, 12.5 and 25 μg/mL, respectively. Then 5 mg/mL^{-1} stock solution of MTT [3-(4,5-dimethylthiazol-2-yl)-2,5-diphenyltetrazolium bromide] was prepared in PBS and this stock solution (20 μL) was added to each well. The plates were incubated at 37 °C for 4 h. Then, the medium containing MTT was removed and dimethyl sulfoxide (DMSO, 150 μL) was added to each well to dissolve the MTT formazan crystals. Finally, the plates were shaken on a shaking table at 150 rpm for 15 minutes, to thoroughly mix the formazan into the solvent. The absorbance of the suspension was recorded at 490 nm by a microplate reader (Thermo Multiskan MK3). Meanwhile, the biocompatibility of the sample was also determined using MTT assay on HeLa cells, which was the same as the procedures for cytotoxicity assay.

2.6. Cellular uptake

Cellular uptake was examined by using confocal laser scanning microscope (CLSM). The HeLa cells were seeded in 6-well culture plates and grown overnight as a monolayer and were incubated with CMC-Er@Yb@Nd@Gd（145.3 mg/mL）at 37 ° C for different periods (10 min, 3 h and 6 h), respectively. Thereafter, the cells were rinsed with phosphoric acidic buffer solution (PBS) three times, fixed with 2.5% formaldehyde (1 mL/well) at 37 °C for 10 min, and then rinsed with PBS three times again. In order to label the nucleus, the nuclei were stained with DAPI (1 mL/well) for 10 min and then rinsed with PBS three times. The coverslips were placed on a glass microscope slides, and the samples were visualized using CLSM.

2.7. Magnetic resonance imaging

2.7.1. Magnetic resonance imaging in aqueous solution.

The longitudinal relaxation time T_1 and relaxivity r_1 of the CMC-Er@Yb@Nd@Gd were performed on a 1.2 T MRI instrument. A series of samples with different Gd^{3+} concentrations in aqueous solution were placed in 1.5 mL tubes for T_1 measurement. The relaxivity r_1 was obtained by plotting $1/T_1$ (s^{-1}) vs. molar concentration of Gd^{3+} (mM).

2.7.2. Magnetic resonance imaging in cell.

HeLa cells were seeded onto 6 well plates at a density of $3x10^5$ cells per well at 37 °C under 5% CO_2 overnight. Then, different concentrations of CMC-Er@Yb@Nd@Gd dispersion (0, 0.125, 0.25, 0.5, 1 and 2 mM) diluted in DMEM without serum were added. After 24 h, the cells were washed three times with PBS to remove free nanoparticles and digested by the addition of 1 mL of trypsin without ethylenediaminetetraacetic acid (EDTA) solution (0.25%). After centrifugation (1500 rpm, 5 min), HeLa cells containing CMC-Er@Yb@Nd@Gd in PBS were precipitated at the bottom of the centrifuge tube. The MR imaging experiments were performed on a 1.2 T MRI instrument.

2.8. Characterization

X-Ray power diffraction (XRD) was performed on a D8 Focus diffractometer (Bruker) with Cu Ka radiation (λ= 0.15405 nm). Transmission electron microscopy (TEM) was performed using FEI Tecnai G2 S-Twin with a field emission gun operating at 200 kV. Images were acquired digitally on a Gatan multiople CCD camera. Fourier-transform IR spectra were recorded on a Perkine Elmer 580B IR spectrophotometer using KBr pellet technique. The UC emission spectra were obtained by using a 808 nm laser diode. The MR imaging experiments were performed on a 1.2 T MRI instrument.

3 Results and Discussion

3.1. Designs of water-soluble CMC-Er@Yb@Nd@Gd

The goal of work was to yield 808 nm excited, water-soluble and biocompatible upconversion nanoparticles for MR/UCL imaging and drug carriers. The general synthetic procedure for CMC-Er@Yb@Nd@Gd was illustrated in Scheme. 1. First, oleic acid capped $BaGdF_5$:20%Yb^{3+}/2%Er^{3+}@$BaGdF_5$:10%Yb^{3+}@$BaNdF_5$@$BaGdF_5$ (Er@Yb@Nd@Gd) nanoparticles were synthesized by a high boiling solvent process. To enhance the upconversion luminescence intensity, different shells were constructed around the as-prepared core to form a core/shell/shell/shell structure. Then the hydrophobic Er@Yb@Nd@Gd nanoparticles dissolved in chloroform were transferred into an aqueous medium by using hydrophilic and biocompatible polymer carboxymethyl chitosan (CMC), which endows these NPs with good water solubility. Additionally, in neutral system (pH= 7.4), part of carboxylic acid groups of CMC will associate into negative charges and the other carboxyl groups keep molecular form.[45] As a result, the partly charged carboxyl groups endow CMC-Er@Yb@Nd@Gd with negative zeta potential (-12.85 mV), which can load antitumor DOX with positive charge by electrostatic interactions.

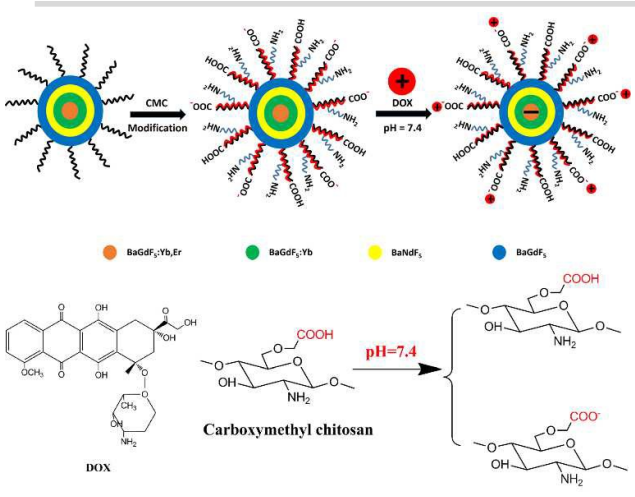

Scheme 1 The design and synthesis of DOX-loaded CMC-Er@Yb@Nd@Gd nanoparticles.

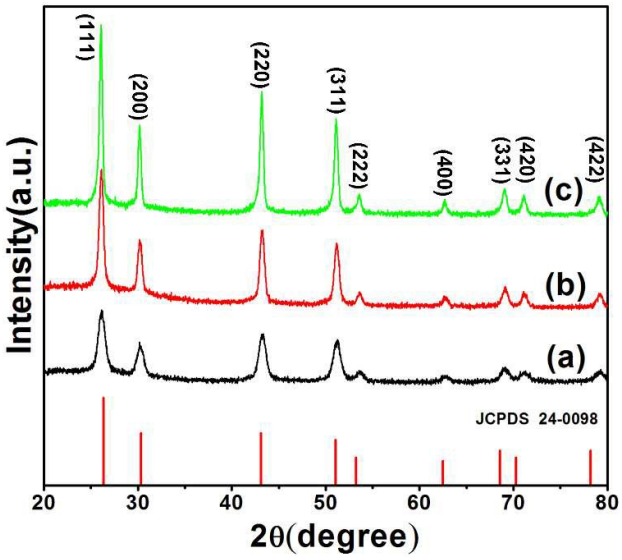

Fig. 1 XRD patterns of (a) $BaGdF_5$:20%Yb^{3+}/2%Er^{3+}, (b) Er@Yb@Nd and (c) Er@Yb@Nd@Gd. (The amount of each shell layer is 0.3 mmol of $BaGdF_5$:10% Yb^{3+}, 0.5 mmol of $BaNdF_5$, and 0.5 mmol of $BaGdF_5$, respectively.)

3.2. Synthesis and characterizations of Er@Yb@Nd@Gd

The XRD patterns of the samples are showed in Fig. 1. All the diffraction peaks can be indexed as a pure cubic phase $BaGdF_5$. Furthermore, the locations and relative intensity of the diffraction peaks coincide well with the literature values (JCPDS NO.24-0098). It can be observed that the peaks are stronger and narrower with the increase of shell thickness, which indicates the nanoparticles have more highly crystalline nature and larger size.

The size and morphology were further examined by transmission electron microscopy (TEM). It can be clearly seen that these NPs have good monodispersity. The size of particles can be tuned from 15 nm to 25 nm. Compared with core (Fig.2a), the size of Er@Yb (Fig.2c) was increased from 15.5 nm to 17 nm, which indicated that the thickness of the shell is about 1.5 nm. Based on Er@Yb nanoparticle, we constructed the Er@Yb@Nd (Fig.2e, 20 nm) and Er@Yb@Nd @Gd (Fig.2g, 25 nm). The corresponding HRTEM images (Fig.2b, d, f, and h) show clearly lattice fringes with planar distance

of 3.488 Å, corresponding to the (111) crystal face of $BaGdF_5$. This also further reveals the highly crystalline nature of as-prepared nanoparticles.

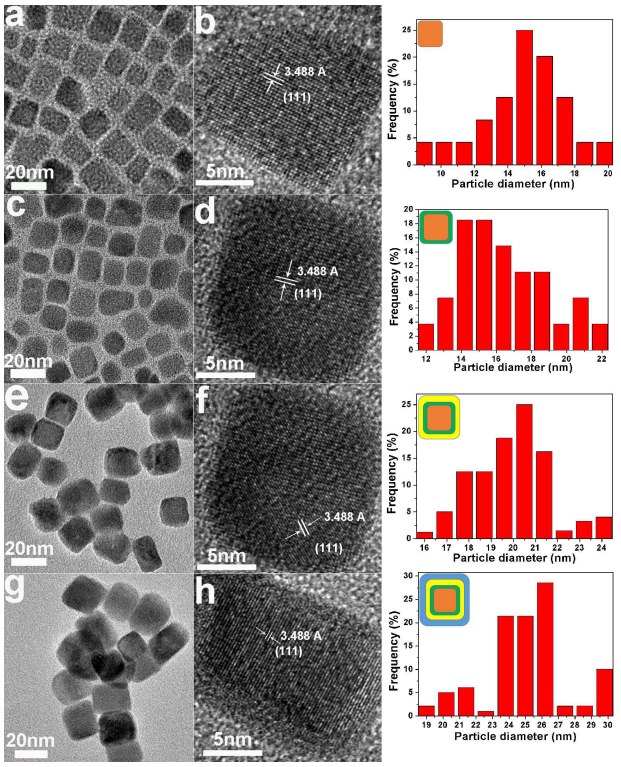

Fig. 2 TEM and HRTEM images of $BaGdF_5$:20%Yb^{3+}/2%Er^{3+} (a, b, 15.5 nm); Er@Yb (c, d, 17 nm); Er@Yb@Nd (e, f, 20 nm) and Er@Yb@Nd @Gd (g, h, 25 nm).

3.3 Optimization and upconversion luminescence properties of Er@Yb@Nd@Gd

In our current systems, Er^{3+} ions (activator) were embedded in the core, Yb^{3+} ions as energy transition layer and Nd^{3+} ions are confined in the second shell layer as the sensitizer to harvest 808 nm photons, resulting in the formation of sandwich structured $BaGdF_5$:20%Yb^{3+}/2%Er^{3+}@$BaGdF_5$:10%Yb^{3+}@$BaNdF_5$ nanoparticles. Under excitation of 808 nm light, the $^4F_{5/2}$ state of Nd^{3+} is populated and the Yb^{3+} ion extracts the excitation energy from the sensitizer Nd^{3+} through interionic cross-relaxation [($^4F_{3/2}$)Nd, ($^2F_{7/2}$)Yb] →[($^4I_{9/2}$)Nd, ($^2F_{5/2}$)Yb]. The excitation-energy migration over the Yb sublattice is followed and finally entrapped by the activator ions Er^{3+} in the inner core. In order to obtain nanoparticles with higher upconversion luminescence intensity, the layer shell $BaGdF_5$ was coated as the outermost layer (Fig. S1, electronic supplementary information). The reaction conditions were optimized elaborately by varying the doping concentration, amount and types of the shells.

The transition layer $BaGdF_5$:10%Yb^{3+} successfully prevented non-radiative resonant energy transfer from activator Er^{3+} to sensitizer Nd^{3+}. It can suppress the detrimental relaxation pathways obviously by increasing the interionic distance between these two ions. The excitation energy could be transferred from the sensitizer Nd^{3+} to the activator Er^{3+} through the transition layer with a certain amount of Yb^{3+} dopant. The transition layer has the role of shield to prevent quenching interactions between Er^{3+} and Nd^{3+}, while energy can be still transferred from Nd^{3+} to Er^{3+} efficiently through the core–shell–shell interface. For a given energy transfer between two lanthanide ions, it depends largely on the distance between donor and acceptor.[46] Therefore, the thickness of the transition layer plays an important role in the efficacy of its shielding. By modulating the amount of the transition layer (n = 0, 0.1, 0.2, 0.3 and 0.5 mmol), the UC emission of $BaGdF_5$:20%Yb^{3+}/2%Er^{3+}@$BaGdF_5$:10%Yb^{3+}@ $BaNdF_5$ increased as the distance between sensitizer layer and activator layer added when excited with 808 nm light (Fig. 3a). The emission intensity reaches a maximum when the thickness of the transition layer is about 1.5 nm (n = 0.3 mmol). It was found that the UC luminescence intensity of $BaGdF_5$:10%Yb^{3+} with doping concentration 0.3 mmol has increased 3.5 times compared with that of nanoparticles in the absence of transition layer.

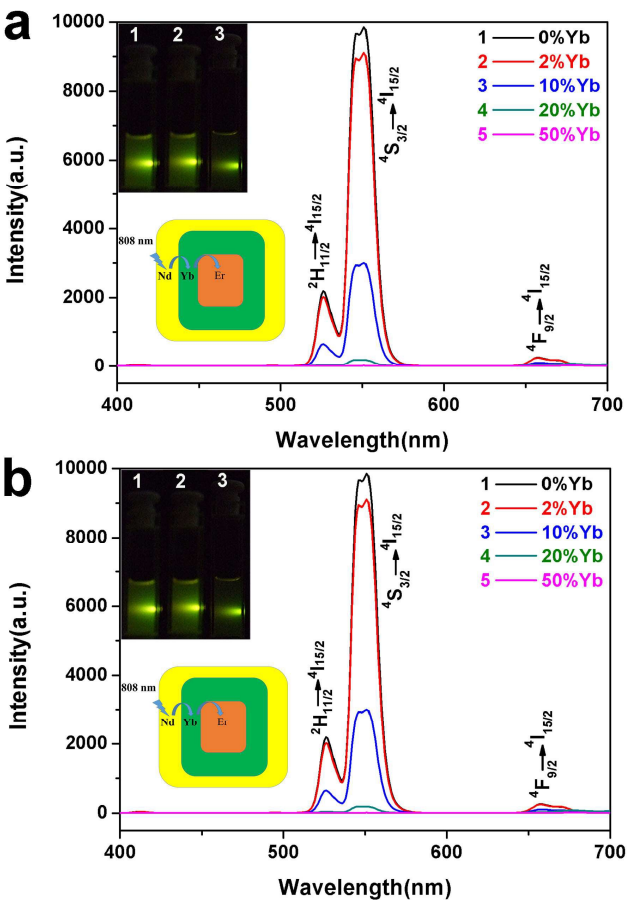

Fig. 3 The upconversion emission spectra and digital photographs (inset) of (a) $BaGdF_5$:20%Yb^{3+}/2%Er^{3+}@y$BaGdF_5$:10%Yb^{3+}@$BaNdF_5$ (y=0, 0.1, 0.2, 0.3 and 0.5 mmol) and (b) $BaGdF_5$:20%Yb^{3+}/2%Er^{3+}@$BaGdF_5$:10%Yb^{3+}@ $BaNdF_5$:x%Yb^{3+} (x=0, 2, 10, 20 and 50) under the excitation of 808 nm.

Next, based on the above optimized conditions, we studied the effects of the doping concentration of Yb^{3+} ions in the second shell layer $BaNdF_5$:Yb^{3+} on the luminescence intensity. When all the other conditions remain unchanged, a series of $BaGdF_5$:20%Yb^{3+}/2%Er^{3+}@$BaGdF_5$:10%Yb^{3+}@$BaNdF_5$:x%Yb^{3+} with different doping concentration of Yb^{3+} ions (x=0, 2, 10, 20, and 50) were fabricated. From Fig. 3b, it can be seen that the upconversion luminescence intensity decreased gradually with the increase of Yb^{3+} doping levels. Moreover, the luminescence intensity was the strongest without Yb^{3+} ion doping in the second shell layer. This demonstrated that Nd^{3+} absorbed 808 nm photon transferred directly the energy to the Yb^{3+} in the transition layer. Increasing concentration of Yb^{3+} in the second shell layer will cause to decrease emission intensity. The unwanted quenching effects resulted from Nd^{3+} ions can be largely avoided with a pure $BaNdF_5$ coating. Namely, the doping concentration of Nd^{3+} in our current systems can up to 100%, which is different from previously reported $NaYF_4$-based nanomaterials.[28] As illustrated in Fig. 3b, the UC intensity of a pure $BaNdF_5$ coating has increased 4 times compared with that of $BaNdF_5$:10%Yb^{3+} as the energy harvest layer. The results confirm that energy can be directly transferred from the Nd^{3+} in the shell layer to the Er^{3+} ions in the core more efficiently through a network of Yb sublattice.

However, when the amount of $BaGdF_5$: 10%Yb^{3+} layer is 0 mmoL and the doping concentrations of Yb^{3+} ions of $BaNdF_5$:Yb^{3+} layer is 20% and 50%, respectively, the upconversion luminescence intensity is too weak to be observed. Therefore, the corresponding luminescence photographs are not showed in Fig. 3a and 3b.

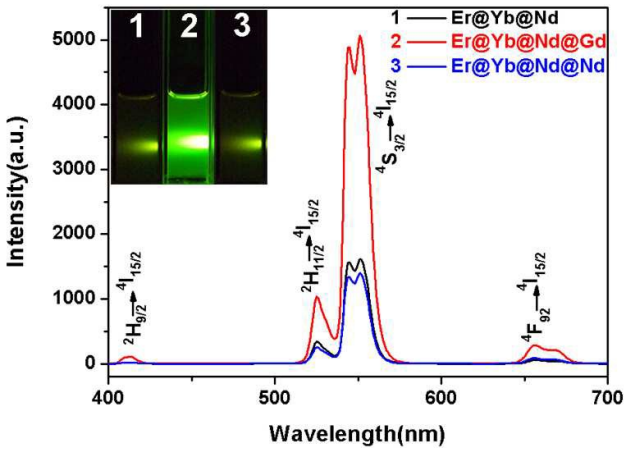

Fig. 4 The upconversion emission spectra and digital photographs (inset) of Er@Yb@Nd, Er@Yb@Nd@Gd and Er@Yb@Nd@Nd. The emission spectra are recorded with an excitation source of 808 nm.

To further enhance the upconversion emission, $BaGdF_5$ layer was coated as the outermost layer to avoid the excitation energy loss. Growing a $BaGdF_5$ layer can prohibit interfacial energy transfer. $BaGdF_5$ layer can effectively enhance UCL through suppressing the surface quenching effects. For coating $BaNdF_5$ as the outermost layer, it is obvious to find the luminescence intensity weakened as a result of the concentration quenching of Nd^{3+}. Cross-relaxation between Nd^{3+} ions is induced when the concentration of Nd^{3+} ion is too high.[47-48] Through cross-relaxation $Nd^{3+}(^4F_{3/2})$ + $Nd^{3+}(^4I_{9/2})\rightarrow$ $Nd^{3+}(^4I_{15/2})$ + $Nd^{3+}(^4I_{15/2})$, the photons populated at the excited state $^4F_{3/2}$ reduce, which decreases the energy transferred to Yb^{3+} and therefore the luminescence intensity of Er^{3+} weakens. Thus, when coating $BaNdF_5$ as the outermost layer, Nd^{3+} ions in the adjacent two layers will produce cross-relaxation phenomena, which weakens the luminescence intensity of Er@Yb@Nd@Nd. Compared with coating $BaNdF_5$ as the outermost layer, it is observed that the UC luminescence intensity of coating a $BaGdF_5$ layer has been enhanced obviously (Fig. 4).

Taken together, $BaGdF_5$:20%Yb^{3+}/2%Er^{3+}@$BaGdF_5$:10%Yb^{3+}@$BaNdF_5$@$BaGdF_5$ nanoparticles with optimized doping concentrations of rare earth ions, amounts and types of the shells were fabricated successfully, which will be used for the following biological experiments.

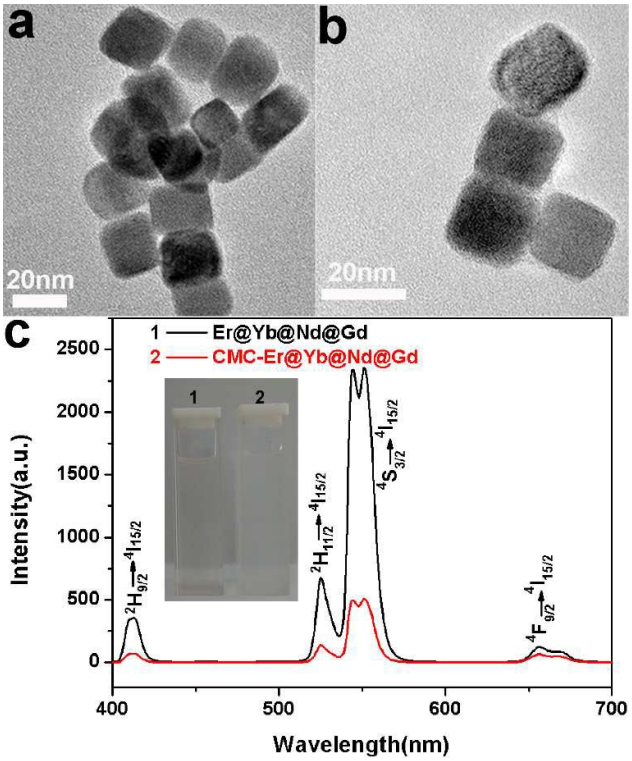

Fig. 5 TEM images of Er@Yb@Nd@Gd (a) before and (b) after transferred into water as well as (c) the corresponding upconversion emission spectra and digital photographs in daylight.

3.4 Characterizations of water-soluble CMC-Er@Yb@Nd@Gd

OA is a hydrophobic molecule and cannot dissolve in physiological environment. CMC has good solubility in water. To improve the biocompatibility and applications in biological field, CMC was conjugated on the surface of UCNPs. After transferred into water by CMC, the average size of Er@Yb@Nd@Gd remains basically

unchanged (Fig. 5a and 5b). Moreover, this transformation process is very effective because there are no visible precipitates in the solution for two days, which can be directly seen from the digital photograph of Er@Yb@Nd@Gd dispersed in chloroform (Fig. 5c-1) and water (Fig. 5c-2). However, the UC luminescence intensity has decreased by 5-fold after transferred into water (Fig. 5c). Green and red upconversion emissions are observed which correspond to the ($^2H_{11/2}$, $^4S_{3/2}$) $\rightarrow$ $^4I_{15/2}$, and $^4F_{9/2}\rightarrow$ $^4I_{15/2}$ transitions, respectively. It can be obviously seen the difference of the relative ratios of red and green emission bands (I_{red} /I_{green}). I_{red} /I_{green} of UCNPs in cyclohexane and water was 0.05 and 0.19, respectively. The quenching of upconversion luminescence is due to water vibrational modes. H_2O solvent molecules with large vibrational modes (≈ 3600 cm^{-1}) produce an increased nonradiative relaxation of the $^4I_{11/2} \rightarrow {}^4I_{13/2}$[49] resulting in a relative increase of the red emission relative to the green emission. The CMC ligands cannot effectively shield the NPs from solvent H_2O molecules. These high energy vibrational modes of the solvent molecules result in an increased nonradiative relaxation of the excited states and thus an overall quenching of the luminescence.

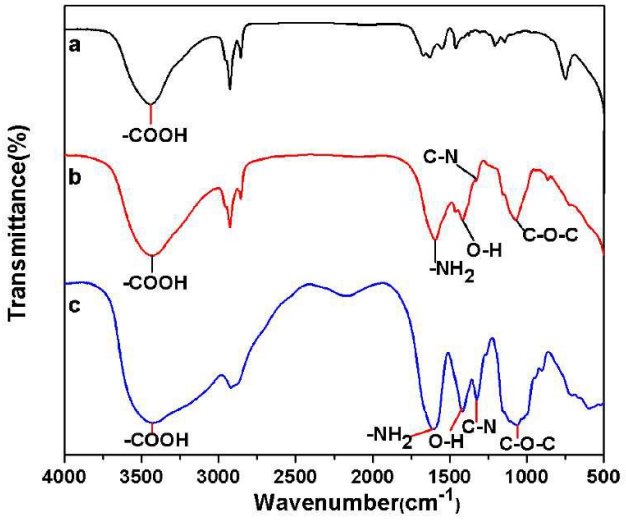

Fig. 6 FT-IR spectra of (a) OA-Er@Yb@Nd@Gd, (b) CMC-Er@Yb@Nd@Gd and (c) pure CMC.

FT-IR spectrum was used to characterize the successful transformation. Fig. 6 shows the FT-IR spectra for OA-Er@Yb@Nd@Gd, CMC-Er@Yb@Nd@Gd and pure CMC, respectively. As shown in Fig. 6c, a peak at 1100 cm^{-1} attributed to the C-O-C stretching vibration while the peaks at 1597-1650 cm^{-1} and 1414-1401 cm^{-1} corresponded to the carboxyl group (which overlaps with N–H bending) and -CH_2COOH group. Compared with Fig. 6a, in the FT-IR spectrum of CMC-Er@Yb@Nd@Gd (Fig. 6b), the characteristic peaks at 1100 cm^{-1}, 1597-1650 cm^{-1} and 1414-1401 cm^{-1} of CMC attributes to C-O-C stretching vibration, –COOH and –NH_2 bending vibrations strengthened obviously. On the characteristic spectrum of CMC modified NCs, the peaks situated at 1325 cm^{-1} and 1420 cm^{-1} in pure CMC corresponding to the C–N of the –NH_2 group and O-H bending weakened respectively. The above results indicated the successful modification of CMC.[50]

3.5 In vitro toxicity

It is essential to evaluate the biocompatibility of the materials for their potential biological applications. The CMC-Er@Yb@Nd@Gd with a range of dosages was chosen to test cytotoxicity based on MTT assay. It shows the in vitro cell viability of CMC-Er@Yb@Nd@Gd with different concentrations ranging from 3.125 to 200 μg/mL for 24 h (Fig. S2, electronic supporting information). These UCNPs exhibited good cell viability, where more than 100% cell viability was observed after incubation at a high dose concentration (200 μg/mL) for 24 h. The data show the CMC modified nanoparticles have favourable biocompatibility in vitro.

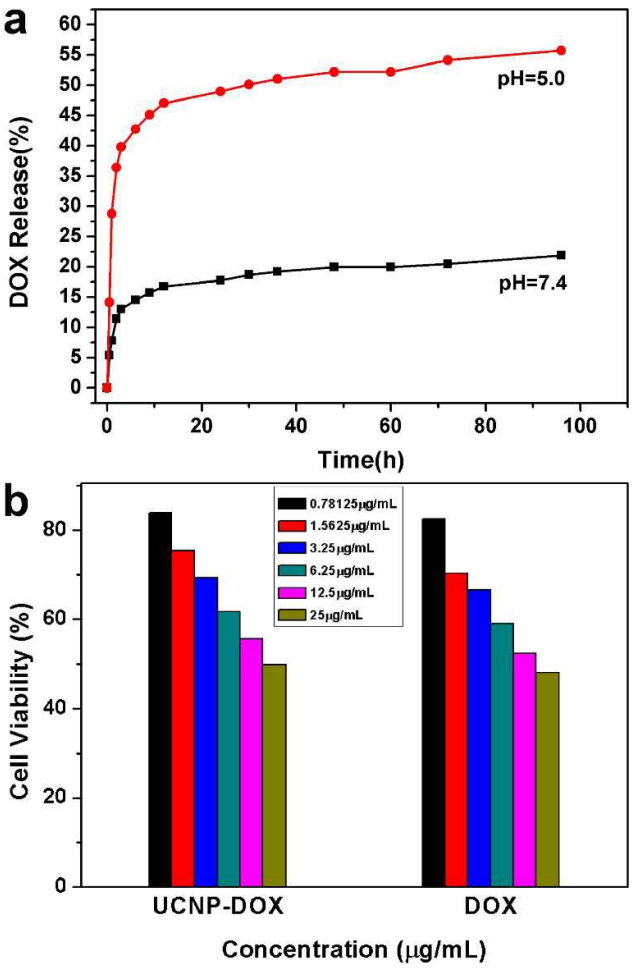

Fig. 7 (a) Cumulative DOX release from DOX-CMC-Er@Yb@Nd@Gd as functions of release time in the release media of PBS buffer with different pH values and (b) In vitro cytotoxicity of free DOX and DOX-CMC-Er@Yb@Nd@Gd against HeLa cells after 24 h incubation.

3.6 Controlled drug release behavior

We further examined the drug delivery property. The drug loading content of DOX is calculated to be 9.2% according to the characteristic DOX optical absorbance at 480 nm. The DOX release profiles of the DOX-CMC-Er@Yb@Nd@Gd in phosphate buffer (PBS) at different pH values (7.4 and 5.0) at 37°C are shown in Fig. 7a. It can be seen that the drug release rate was obviously pH dependent and increased with the decrease of pH. The cumulative DOX release was only 20.0% even after 48 h at pH 7.4. Considering the acidic environment of tumor tissue, PBS (pH = 5.0) was used to simulate the intracellular conditions of cancer cells. The DOX release rate reaches to 52.2% after 48 h. This pH triggered drug release behavior can be explained as follows: CMC exists in the acidic environment in molecular form. Therefore, the surface of the nanoparticles exists few negative charges and DOX can be released because of the weak electrostatic interaction. On the other hand, owing to the increased number of protonated NH_2 groups on DOX with lower pH, the hydrophilicity and solubility of DOX improved, which results in drug release. However, DOX is relatively stable in normal physiological environment. The pH-sensitive DOX release might be beneficial at the reduced pH values in certain cancerous tissues for targeted release and controlled therapy at the pathological sites.[51]

To test the pharmacological activity of DOX-CMC-Er@Yb@Nd@Gd, the cytotoxic effects on HeLa cells were evaluated in vitro by MTT assay. HeLa cells were incubated in culture medium containing free DOX and DOX-CMC-Er@Yb@Nd@Gd for 24 h at different DOX concentrations. Fig. 7b shows the DOX-CMC-Er@Yb@Nd@Gd had comparable cytotoxicity with free DOX at the same concentration of DOX, which shows an increasing inhibition against HeLa cells with the increase of concentration. This suggests that CMC-Er@Yb@Nd @Gd is an efficient drug delivery vehicle.

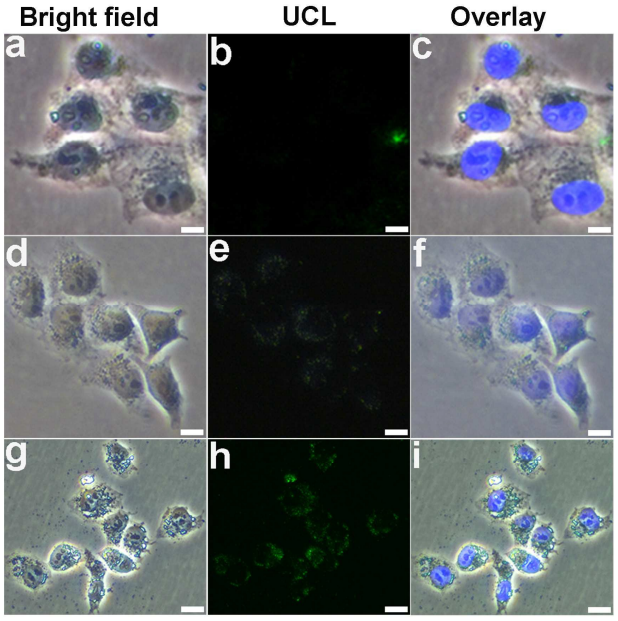

Fig. 8 Inverted fluorescence microscope images of HeLa cells incubated with CMC-Er@Yb@Nd@Gd nanoparticles 30 min (a–c), 3 h (d-f) and 6 h (g-i) at 37 °C. The scale bar is 25 μm.

3.7 Cell uptake

Cellular-uptake of nanoparticles are investigated by using upconversion luminescence imaging. In order to further verify that nanomaterials can be internalized by the cells, the upconversion bioimaging was done by utilizing modified inverted fluorescence microscopy equipped with infrared laser excitation at 808 nm. After CMC-Er@Yb@Nd@Gd (200 μg/mL) were incubated with HeLa cells at 37 °C for 30 min, 3 h, and 6 h, the obvious UCL signal can be observed from the HeLa cells under the excitation of a 808 nm laser (Fig. 8). It showed that more and more nanoparticles were internalized into the cells with increasing time. This indicates that CMC-Er@Yb@Nd@Gd can be used as an excellent luminescence probe for cell imaging and monitoring the cell endocytosis process. When the tumors grew for around 6 days, NPs were injected into the tumor in situ. As shown in Fig. S4, the bright green emission can be clearly observed, which suggested that the NPs can be used to conduct living imaging.

3.8 MR imaging

It is well known that Gd^{3+} has isotropic electronic ground state $^8S_{7/2}$ and half-filled f-orbital with seven electrons.[52] Gd^{3+}-based nanoparticles have potential as MRI contrast agents because of their positive signal-enhancement ability. To examine the MR property of the as-prepared CMC-Er@Yb@Nd@Gd, the in vitro T_1-weighted MR imaging for CMC-Er@Yb@Nd@Gd was measured. Fig. 9b and 9c show the T_1-weighted MR images were brightened with the increase of Gd^{3+} concentration. From the slope of the line (Fig. 9a), the longitudinal relaxivity (r_1) was determined to be 43.77 s^{-1}

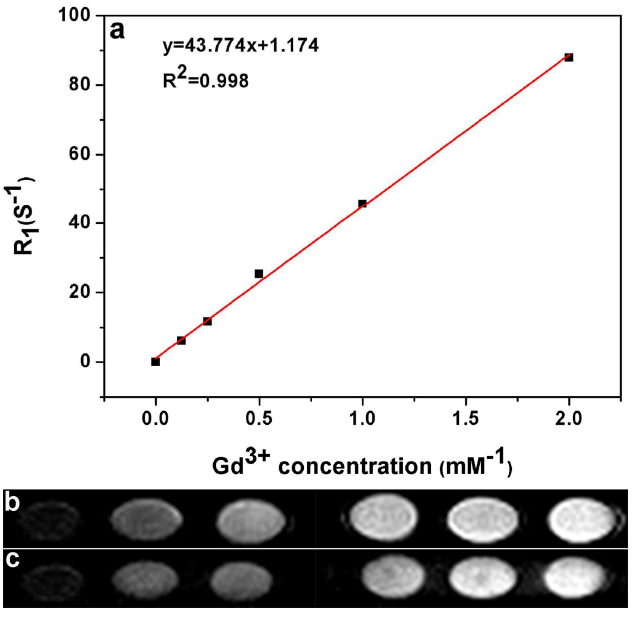

Fig. 9 (a) Deionized water (0 mM) was the reference. Plots of relaxation rate r_1 ($1/T_1$) as a function of Gd concentration at room

temperature using a 1.2 T MRI scanner; T_1-Weighted MR images for various Gd concentrations of CMC-Er@Yb@Nd@Gd (b) in solution and (c) in cells.

$(mM)^{-1}$, which is enhanced by 10 times compared with 4.11 s^{-1} $(mM)^{-1}$ in Yang's work.[44] It may be explained as follows: The shorter distance between contrast agents and hydrogen nucleus in water can shorten T_1 values. The sample has increased specific surface area, which contributes to the adequate interactions between nanoparticles and hydrogen nucleus. Therefore, the longitudinal relaxivity (r_1) increased. The in vitro results indicate that the CMC-Er@Yb@Nd@Gd may serve as an efficient T_1-weighted MRI contrast agents.

4 Conclusions

In conclusion, we have designed 808 nm excited $BaGdF_5$:20%Yb^{3+}/2%Er^{3+}@$BaGdF_5$:10%Yb^{3+}@$BaNdF_5$@$BaGdF_5$ core/shell/shell/shell structured upconversion nanoparticles (Er@Yb@Nd@Gd) with the size of about 25 nm. In contrast to $BaGdF_5$:20%Yb^{3+}/2%Er^{3+}@$BaGdF_5$:10%Yb^{3+}@$BaNdF_5$, the UC luminescence intensity is improved more than 4 times after coating a $BaGdF_5$ layer. Biocompatible and hydrophilic CMC is used as a phase transfer agent to transfer hydrophobic UCNPs into aqueous solution for bioimaging and loading of antitumor drug DOX. Er@Yb@Nd@Gd exhibited enhanced NIR-to-Vis luminescence property. In vitro cell cytotoxicity tests revealed that Er@Yb@Nd@Gd exhibit good biocompatibility and low toxicity. Moreover, upconversion fluorescence signals from CMC-Er@Yb@Nd@Gd were observed over the cell membrane under 808 nm NIR light excitation. The doping of Gd^{3+} makes the NPs with a high relaxivity of 43.77 s^{-1} $(mM)^{-1}$, demonstrating good MRI effect. Subsequently, DOX in CMC- Er@Yb@Nd@Gd can be released in pH-sensitive pattern, which helps decrease the amount of DOX released in normal tissues and reduce the side-effect of chemotherapeutics. Thus, these UCNPs combine the features with optical/MR bimodal imaging capabilities and drug delivery for chemotherapeutics.

Acknowledgements

This project is financially supported by the National Natural Science Foundation of China (NSFC 51332008, 51372243, 51422209, 51572258, 51472233), National Basic Research Program of China (2014CB643803).

Notes and references

1 F. Wang and X. G. Liu, *Chem. Soc. Rev.*, 2009, **38**, 976.
2 W. Y. Yin, L. N. Zhao, L. J. Zhou, Z. J. Gu, X. X. Liu, G. Tian, S. Jin, L. Yan, W. L. Ren, G. M. Xing and Y. L. Zhao, *Chem. Eur. J.*, 2012, **18**, 9239.
3 Y. Wu, D. M. Yang, X. J. Kang, Y. Zhang, S. S. Huang, C. X. Li and J. Lin, *CrystEngComm*, 2014, **16**, 1056.
4 W. P. Qin, Z. Y. Liu, C. N. Sin, C. F. Wu, G. S. Qin, Z. Chen and K. Z. Zheng, *Light: Sci. Appl.*, 2014, **3**, 193.
5 G. Y. Chen, H. Ågren, T. Y. Ohulchanskyya and P. N. Prasad, *Chem. Soc. Rev.*, 2015, **44**, 1680
6 Q. Liu, B. R. Yin, T. S. Yang, Y. C. Yang, Z. Shen, P. Yao and F. Y. Li, *J. Am. Chem. Soc.*, 2013, **135**, 5029.
7 G. Tian, Z. J .Gu, L. J. Zhou, W. Y. Yin, X. X. Liu, L. Yan, S. Jin, W. L. Ren, G. M. Xing, S. J. Li and Y. L. Zhao, *Adv. Mater.*, 2012, **24**, 1226.
8 Y. Il. Park, K. T. Lee, Y. D. Suh and T. Hyeon, *Chem. Soc. Rev.*, 2015, **44**, 1302.
9 A. Sedlmeier and H. H. Gorris, *Chem. Soc. Rev.*, 2015, **44**, 1526.
10 B. Liu, Y. Y. Chen, C. X. Li, F. He , Z. Y. Hou , S. S. Huang , H. M. Zhu, X. Y. Chen and J. Lin, *Adv. Funct. Mater.*, 2015, **25**, 4717.
11 M. -H. Kim, H. -K. Na, Y. -K. Kim, S. -R. Ryoo, H. S. Cho, K. E. Lee, H. Jeon, R. Ryoo and D. –H. Min, *ACS Nano*, 2011, **5**, 3568.
12 S. L. Gai, C. X. Li, P. P. Yang and J. Lin, *Chem. Rev.*, 2014, **114**, 2343.
13 N. M. Idris, M. K. Gnanasammandhan, J. Zhang, P. C. Ho, R. Mahendran and Y. Zhang, *Nat. Med.*, 2012, **18**, 1580.
14 J. Zhou, Z. Liu and F. Y. Li, *Chem. Soc. Rev.*, 2012, **41**, 1323.
15 H. Dong, L. D. Sun and C. H.Yan, *Nanoscale.*, 2013, **5**, 5703.
16 F. Wang, L. D. Sun, J. Gu , Y. F. Wan, W. Feng, Y. Yang, J. F. Wang and C. H. Yan, *Angew. Chem. Int. Ed.*, 2012, **51**, 8796.
17 G. Y. Chen, J. Shen, T. Y. Ohulchansky, N. J. Patel, A. Kutikov, Z. P. Li, J. Song, R. K. Pandey, H. Ågren, P. N. Prasad and G. Han, *ACS Nano*, 2012, **6**, 8280.
18 L. Cheng, K. Yang, Y. G. Li, J. H. Chen, C. Wang, M. W. Shao, S. -T. Lee and Z. Liu, *Angew. Chem. Int. Ed.*, 2011, **50**, 7385.
19 F. Zhang, G. B. Braun, A. Pallaoro, Y. C. Zhang, Y. F. Shi, D. X. Cui, M. Moskovits, D. Y. Zhao and G. D. Stucky, *Nano Lett.*, 2012, **12**, 61.
20 D. E. Achatz, R. J. Meie, L. H. Fische and O. S. Wolfbeis, *Angew. Chem. Int. Ed.*, 2011, **50**, 260.
21 F. Wang, R. Deng, J. Wang, Q. Wang, Y. Han, H. Zhu, X. Chen and X. Liu, *Nat. Mater.*, 2011, **10**, 968.
22 Y. F. Wang, G. Y. Liu, L. D. Sun, J. W. Xiao, J. C. Zhou and C. H. Yan, *ACS Nano*, 2013, **7**, 7200.
23 X. J. Xie, N. Y. Gao, R. R. Deng, Q. Sun, Q. H. Xu and X. G. Liu, *J. Am. Chem. Soc.*, 2013, **135**, 12608.
24 H. L. Wen, H. Zhu, X. Chen, T. F. Hung, B. L. Wang, G. Y. Zhu, S. F. Yu and F. Wang, *Angew. Chem. Int. Ed.*, 2013, **52**, 13419.
25 P. Huang, W. Zheng, S. Y. Zhou, D. T. Tu, Z. Chen, H. M. Zhu, R. F. Li, E. Ma, M. D. Huang and X. Y. Chen, *Angew. Chem. Int. Ed.*, 2014, **53**, 1252.
26 T. Q. Wu, M. Barker, K. M. Arafeh, J. -C. Boyer, C. -J. Carling and N. R. Branda, *Angew. Chem. Int. Ed.*, 2013, **52**, 11106-11109.
27 Q. Q. Zhan, J. Qian, H. J. Liang, G. Somesfalean, D. Wang, S. L. He, Z. G. Zhang and S. Andersson-Engels, *ACS Nano*, 2011, **5**, 3744.
28 Y. T. Zhong, G. Tian, Z. J. Gu , Y. J.Yang, L. Gu, Y. L. Zhao ,Y. Ma and J. N. Yao, *Adv. Mater.*, 2014, **26**, 2831.
29 X. Y. Huang and J. Lin, *J. Mater. Chem. C*, 2015, **3**, 7652.
30 K. Wang, W. Li, Q. Cheng, Y. Zhang, R. Qiao, S. Li and Z. Q. Li, *RSC Adv.*, 2015, **5**, 62899.
31 Y. Y. Chen，P. A. Ma, D. M. Yang, Y. Wu, Y. L. Dai, C. X. Li and J. Lin, *Chem. Asian J.*, 2014, **9**, 506.
32 L. J. Zhou, Z. J. Gu, X. X. Liu, W. Y. Yin, G. Tian, L. Yan, S. Jin, W. L. Ren, G. M. Xing, W. Li, X, L. Chang, Z. B. Hu and Y, L, Zhao, *J. Mater. Chem.*, 2012, **22**, 966.
33 S. Setua, D. Menon, A. Asok, S. Nair and M. Koyakutty, *Biomaterials*, 2010, **31**, 714.
34 J. Zhou, Y. Sun, X. X. Du, L. Q. Xiong, H. Hu and F. Y. Li, *Biomaterials*, 2010, **31**, 3287.
35 J. Zhou, M. X. Yu, Y. Sun, X. Z. Zhang, X. J. Zhu, Z. H. Wu, D. M. W and F. Y. Li, *Biomaterials*, 2011, **32**, 1148.
36 G. Tian, Z. J. Gu, X. X. Liu, L. J. Zhou, W. Y. Yin, L. Yan, S. Jin, W. L. Ren, G. M. Xing, S. J. Li and Y. L. Zhao, *J. Phys. Chem. C.*, 2011, **115**, 23790.
37 R. Liu, Y. L. Guo, G. Odusote, F. L. Qu and R. D. Priestley, *ACS Appl. Mater. Interfaces*, 2013, **5**, 9167.

38 D. L. Ma, J. W. Guan, F. Normandin, S. Denommee, G. Enright, T. Veres and B. Simard, *Chem. Mater.*, 2006, **18**, 1920.
39 Q. L. Ma, J. X. Wang, X. T. Dong, W. S. Yu, G. X. Liu and J. Xu, *J. Mater. Chem.*, 2012, **22**, 14438.
40 B. Q. Lu, Y. J. Zhu, H. Y. Ao, C. Qi and F. Chen, *ACS Appl. Mater. Interfaces*, 2012, **4**, 6969.
41 E. Peng, E. S. G. Choo, C. S. H. Tan, X. S. Tang, Y. Sheng and J. M. Xue, *Nanoscale*, 2013, **5**, 5994.
42 Y. T. Chen, F. Guo, Y. Qiu, H. Hu, I. Kulaots, E. Walsh and R. H. Hurt, *ACS Nano*, 2013, **7**, 3744.
43 F. Y. Liu, X. X. He, L. Liu, H. P. You, H. M. Zhang and Z. X. Wang, *Biomaterials*, 2013, **34**, 5218.
44 D. M. Yang, Y. L. Dai, J. H. Liu, Y. Zhou, Y. Y. Chen, C. X. Li, P. A. Ma and J. Lin , *Biomaterials*, 2014, **35**, 2011.
45 A. P. Zhu, L. H. Yuan and T. Q. Liao, *Int. J. Pharmaceut.*, 2008, **350**, 361.
46 (a) B. Zhou, W. F. Yang, S. Y. Han, Q. Sun and X. G. Liu, *Adv. Mater.*,2015, DOI: 10.1002/adma.201503482; (b) F. R. Cheng, Z. G. Xia, X. P. Jing and Z. Y. Wang, *Phys. Chem. Chem. Phys.*, 2015, **17**, 3689-3696; (c) Z. G. Xia, Y. Luo, M. Guan and L. B. Liao, *Optics Express*, 2012, **20**, A722-A728.
47 T. Kushida, H. M. Marcos and J. E. Geusic, *Phys. Rev.*, 1968, **167**, 289.
48 D. Wang, B. Xue, X. G. Kong, L. P. Tu, X. M. Liu, Y. L. Zhang, Y. L. Chang, Y. S. Luo, H. Y. Zhao and H. Zhang, *Nanoscale*, 2015, **7**, 190.
49 J. C. Boyer, M. P. Manseau, J. I. Murray and F. C. J. M. van Veggel, *Langmuir*, 2010, **26**, 1157.
50 S. Shen, F. F. Kong, X. M. Guo, L. Wu, H. J. Shen, M. Xie, X. S. Wang, Y. Jin and Y. R. Ge, *Nanoscale*, 2013, **5**, 8056.
51 W. Wei, G. H. Ma, G. Hu, D. Yu, T. Mcleish, Z. G. Su and Z. Y. Shen, *J.Am.Chem. Soc*., 2008, **130**, 15808.
52 C. Burtea, S. Laurent, L.V. Elst and R. N. Muller, *Handbook Exp Pharmacol*, 2008, **185**,135.

Graphic abstract

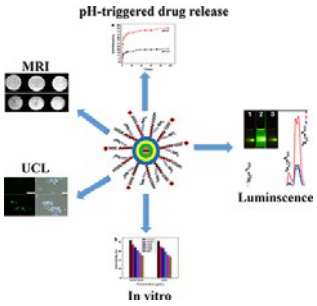

Nd^{3+}-sensitized $BaGdF_5$:20%Yb^{3+}/2%Er^{3+}@$BaGdF_5$:10%Yb^{3+}@$BaNdF_5$@$BaGdF_5$ nanoparticles for dual-model imaging and pH-triggered drug release.